BURBANK, R. D. (1964). *Acta Cryst.* **17**, 434–442.
BUSING, W. R. & LEVY, H. A. (1967). *Acta Cryst.* **22**, 457–464.
DENNE, W. A. (1977*a*). *Acta Cryst.* A**33**, 438–440.
DENNE, W. A. (1977*b*). *Acta Cryst.* A**33**, 987–992.
EINSTEIN, J. R. (1974). *J. Appl. Cryst.* **7**, 331–344.
FIELD, J. E. & LINDSAY, G. A. (1937). *Phys. Rev.* **51**, 165–169.
FREEMAN, D. K., MAIR, S. L. & BARNEA, Z. (1977). *Acta Cryst.* A**33**, 355–359.
FURNAS, T. C. & HARKER, D. (1955). *Rev. Sci. Instrum.* **26**, 449–453.
GAY, P., HIRSCH, P. B. & KELLAR, J. N. (1952). *Acta Cryst.* **5**, 7–11.
HAMILTON, W. C. (1974*a*). In *International Tables for X-ray Crystallography*, Vol. IV, §3.2. Birmingham: Kynoch Press.
HAMILTON, W. C. (1974*b*). In *International Tables for X-ray Crystallography*, Vol. IV, §3.3.2. Birmingham: Kynoch Press.
HARADA, J., PEDERSEN, T. & BARNEA, Z. (1970). *Acta Cryst.* **26**, 336–344.
HOLLENBERG, W. C. & BATTERMAN, B. W. (1974). *Phys. Rev. B*, **10**, 2148–2158.
HUIJSER-GERITS, E. M. C. & RIECK, G. D. (1974). *J. Appl. Cryst.* **7**, 286–290.
KHEIKER, D. M. (1969). *Acta Cryst.* A**25**, 82–88.
LADELL, J., PARRISH, W. & TAYLOR, J. (1959). *Acta Cryst.* **12**, 561–567.
LADELL, J. & SPIELBERG, N. (1966). *Acta Cryst.* **21**, 103–118.
LIMINGA, R., CHOMNILPAN, S. & ABRAHAMS, S. C. (1978). *J. Appl. Cryst.* **11**, 128–131.
MCINTYRE, G. J. (1981). In preparation.
MCINTYRE, G. J. & BARNEA, Z. (1978). *Acta Cryst.* A**34**, S336.
MAIR, S. L. & BARNEA, Z. (1975). *J. Phys. Soc. Jpn*, **38**, 866–869.
MAIR, S. L., PRAGER, P. & BARNEA, Z. (1971*a*). *J. Appl. Cryst.* **4**, 169–171.
MAIR, S. L., PRAGER, P. & BARNEA, Z. (1971*b*). *Nature (London)*, **234**, 35.
MATHIESON, A. MCL. (1975). *Acta Cryst.* A**31**, 769–774.
MATHIESON, A. MCL. (1977). *Acta Cryst.* A**33**, 610–617.
MERISALO, M. & JÄRVINEN, M. (1978). *Philos. Mag.* B**37**, 233–240.
MERISALO, M., JÄRVINEN, M. & KURITTU, J. (1978). *Phys. Scr.* **17**, 23–25.
MERISALO, M., PELJO, E. & SOININEN, J. (1978). *Phys. Lett. A*, **67**, 80–82.
SCHULZ, L. (1949). *J. Appl. Phys.* **20**, 1030–1036.
SHARMA, B. L. (1966). *Solid State Electron.* **9**, 728–729.
TENCKHOFF, E. (1970). *J. Appl. Phys.* **41**, 3944–3948.
TRUCANO, P. & BATTERMAN, B. W. (1972). *Phys. Rev. B*, **6**, 3659–3666.
WERNER, S. A. (1972). *Acta Cryst.* A**28**, 143–151.
WHITELEY, B., MOSS, G. & BARNEA, Z. (1978). *Acta Cryst.* A**34**, 130–136.

Acta Cryst. (1981). A**37**, 119–125

High-Resolution Imaging of the Ferroelectric Perovskite $Ba_2Bi_4Ti_5O_{18}$

BY JOHN L. HUTCHISON

Department of Metallurgy and Science of Materials, University of Oxford, Parks Road, Oxford OX1 3PH, England

AND DAVID J. SMITH

High Resolution Electron Microscope, University Engineering Department, Free School Lane, Cambridge CB2 3RQ, England

(*Received* 12 *June* 1980; *accepted* 4 *September* 1980)

Abstract

The ferroelectric material $Ba_2Bi_4Ti_5O_{18}$ has been examined by high-resolution electron microscopy at 200 and 500 kV. With the directly interpretable resolution limit in each case extending to better than 2·5 Å, it was demonstrated that both the *A*-cation and *B*-cation positions could be resolved and, furthermore, that analysis of structural disorder at this level of resolution allowed an explanation of some observed lattice defects. In particular, unit shifts of a perovskite cell along a bismuthate sheet were identified as occurring in the manner previously postulated, and a Burgers vector circuit analysis around a low-angle domain boundary permitted the formulation of a model for the atomic configuration at the boundary. The implications of these observations for the study of perovskites generally are briefly discussed.

Introduction

The layered compound $Ba_2Bi_4Ti_5O_{18}$ is one of a family (Aurivillius, 1949) which are based on a regular

0567-7394/81/010119-07$01.00

intergrowth of perovskite layers with bismuthate sheets. A schematic representation of its structure projected on (110) is shown in Fig. 1: unit-cell parameters are $a = 5{\cdot}514$, $b = 5{\cdot}526$, $c = 50{\cdot}370$ Å. High-resolution electron microscopy of this ferroelectric at 100 kV indicated that the individual A-cation positions of the perovskite lattice could be resolved and that some lattice defects, such as dislocations, could be observed directly (Hutchison, Anderson & Rao, 1975, 1977). However, the resolution limit for directly interpretable structure information of about 3·5–4·0 Å meant, in particular, that the B-cation positions could not be resolved simultaneously, and that reliable information about many other structural defects, which was beyond this resolution limit, could not be obtained.

It is well known that operation at higher voltages potentially offers higher resolution, and this has been demonstrated experimentally in several laboratories with high-voltage microscopes specifically designed for high resolution (Kobayashi *et al.*, 1974; Dietrich *et al.*, 1977; Horiuchi, Matsui, Bando, Katsuta & Matsui, 1978; Cosslett *et al.*, 1979). Furthermore, recent electron-microscopical observations of $Bi_7Ti_4NbO_{21}$ (Horiuchi, Kikuchi & Goto, 1977) and $Bi_2W_2O_9$ (Bando, Watanabe, Sekikawa, Goto & Horiuchi, 1979), at increased resolution, have shown that direct crystal-structure determinations of some layered bismuth compounds are then possible.

In the present paper we describe further observations on $Ba_2Bi_4Ti_5O_{18}$ in which the higher interpretable resolution recently available has enabled interpretations of several types of structural defects. A preliminary account of some of this work has appeared (Hutchison, 1979).

Experimental details

Observations of crystal structure images were made at 200 kV with a JEM 200CX at Oxford, and at 500 kV with the Cambridge University high-resolution electron microscope (HREM) (Nixon *et al.*, 1977; Cosslett, 1980). The former microscope is equipped with a high-resolution objective lens with spherical (C_s) and chromatic (C_c) aberration coefficients of 1·2 and 1·4 mm respectively and a top-entry, double-tilt (±10°) goniometer specimen holder. Optical diffractograms from micrographs of thin amorphous films of silicon have confirmed the calculated position of the first zero of the contrast transfer at Scherzer defocus at *ca* 2·45 Å (Boyes *et al.*, 1979). Furthermore, the Cambridge HREM, which employs a side-entry, double-tilt (±30°) cartridge, has recently demonstrated an interpretable resolution of *ca* 2·2 Å at 500 kV (Cosslett *et al.*, 1979). Therefore, both microscopes could, in principle, provide direct resolution of all projected cation positions in the principal zone axis of interest in $Ba_2Bi_4Ti_5O_{18}$, namely [110]. With either specially modified pointed tungsten filaments at 200 kV, or indirectly-heated lanthanum hexaboride rods (Ahmed & Broers, 1972) at 500 kV, image astigmatism was normally corrected directly from the fluorescent screen, by use of the granularity of the carbon support film, at magnifications in excess of 5×10^5, although micrographs were typically recorded at $3–5 \times 10^5$.

The compound was prepared from an appropriate mixture of Bi_2O_3, TiO_2 and barium carbonate (Hutchison *et al.*, 1977). Some material was crushed under alcohol in an agate mortar and then mounted on a holey carbon film. Thin fragments were sought which could be oriented with [110] exactly parallel to the electron beam as indicated by the selected-area electron diffraction pattern, Fig. 2. Areas of these fragments which protruded over holes in the supporting film were then chosen for imaging.

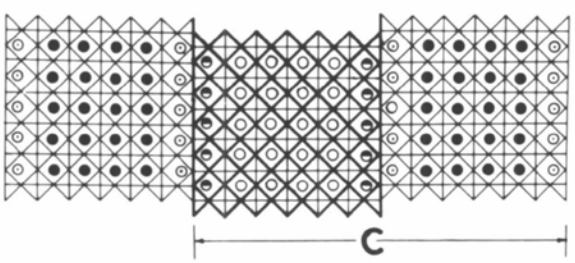

Fig. 1. Schematic structure of $Ba_2Bi_4Ti_5O_{18}$, projected on (110). ⊕ B cations in octahedra at levels $z = 0$ (light lines) and $z = \frac{1}{2}$ (heavy lines); ◓ Bi in Bi_2O_2 layers at $z = 0$; ⊙ Bi in Bi_2O_2 layers at $z = \frac{1}{2}$; ○ A cations at $z = 0$; ● A cations at $z = \frac{1}{2}$.

Observations

The early micrographs of this study were obtained during the commissioning period of the Cambridge 600 kV microscope before its full, high-resolution

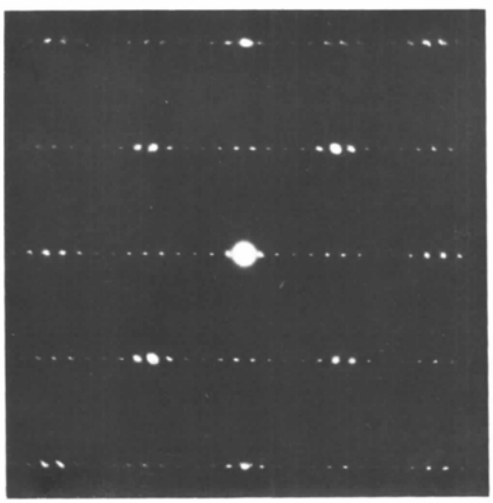

Fig. 2. [110] electron diffraction pattern of $Ba_2Bi_4Ti_5O_{18}$.

performance was realized. Even then, the resolution was at least as good as that obtained previously at 100 kV (Hutchison *et al.*, 1977). Subsequently, images were taken with this microscope fully operational and also with the Oxford JEM 200CX. As already pointed out, both instruments yielded micrographs of $Ba_2Bi_4Ti_5O_{18}$ which showed a marked improvement in resolution compared with previous images of this and related materials (Hutchison, 1979).

This is demonstrated in Fig. 3 which shows structure images of $Ba_2Bi_4Ti_5O_{18}$ in the [110] projection, obtained from both microscopes, with the idealized projection of the structure on the same scale. The slight differences in contrast of the two images are believed to be due to the different shape and extent of the contrast transfer functions of each microscope at optimum defocus. The thickness profiles of the particular crystals are also likely to be different. In Fig. 4, which is an enlarged section of Fig. 3(*a*), the close agreement between image contrast and projected structure is evident. The most prominent feature appears to be the array of white dots which correspond to the oxygen sites in the perovskite sublattice but all cation sites are resolved, which has the side effect of rendering the Bi_2O_2 layers less visible than in lower-resolution images. The good matching between the image and the perfect structure has then enabled us to identify a number of novel defect structures not hitherto observed in such materials, as we now describe.

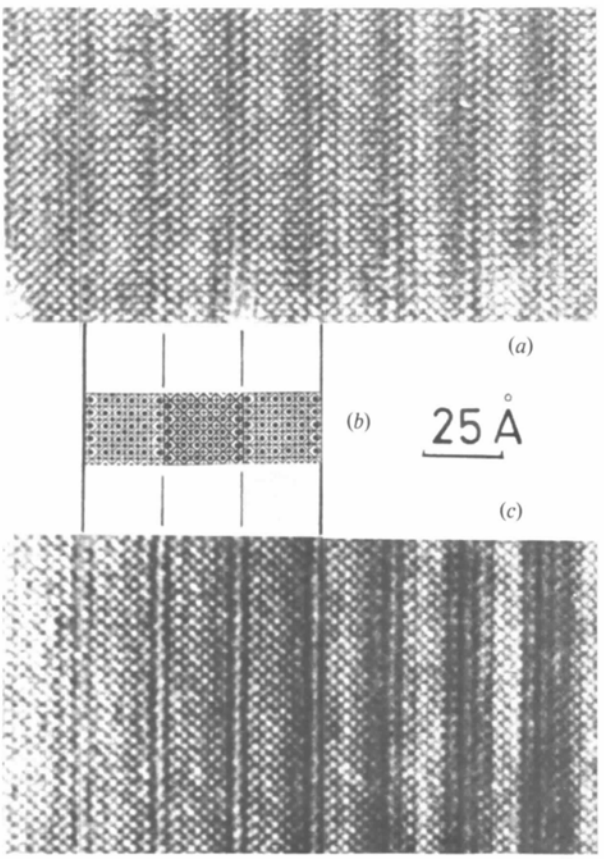

Fig. 3. Structure images of $Ba_2Bi_4Ti_5O_{18}$ along [110]. Taken with (*a*) JEM 200CX and (*c*) Cambridge 600 kV HREM; (*b*) shows the structure of the same scale.

Structure of an antiphase boundary

Fig. 5 shows an early 500 kV image in which the dominant features are the vertical dark lines – the bismuthate layers, and the interleaved square grid of black dots – the *A*-site cations. This micrograph contains a complex antiphase boundary (APB), labelled *AB*.

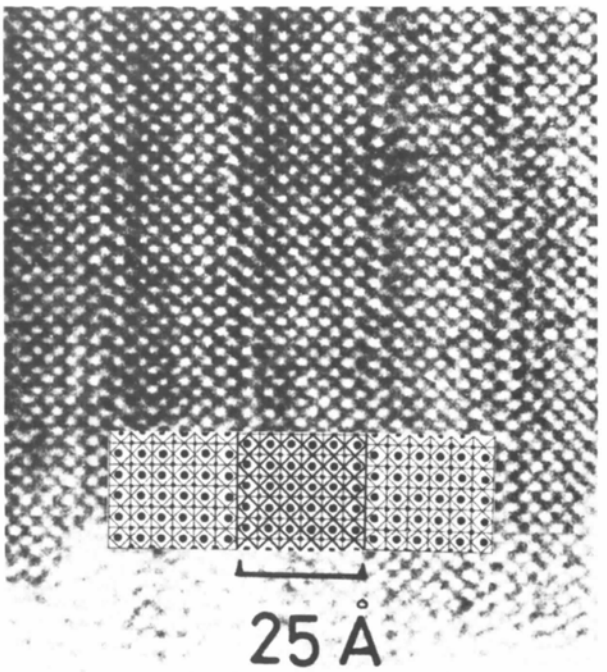

Fig. 4. Enlargement of a part of Fig. 3(*a*) with the structure superimposed.

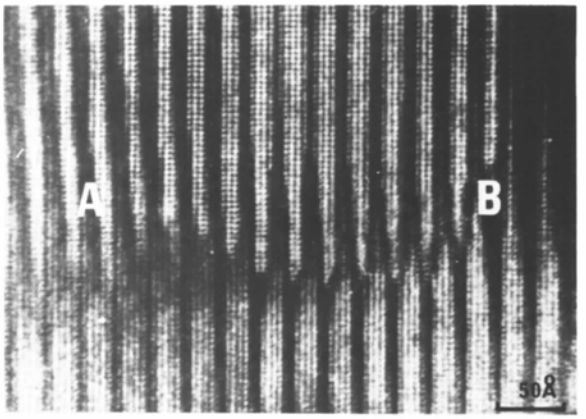

Fig. 5. Early 500 kV image of $Ba_2Bi_4Ti_5O_{18}$ containing a complex antiphase boundary *AB*.

It is possible to deduce a model for this APB because the geometrical constraints in which perovskite layers are held across Bi_2O_2 layers define the relative levels of the octahedra, as well as of the *A*-site cations; these levels must be maintained across any APB. Fig. 6(*a*) illustrates a manner in which this may be done, the most interesting feature of this defect complex being that along the APB the octahedra share edges, which is equivalent to a segment of a (100) crystallographic shear (CS) plane in ReO_3-type structures (*e.g.* Bursill & Hyde, 1972). This is the first evidence for CS fault planes in a perovskite lattice, although an earlier, unsubstantiated claim for '[100] CS' planes in $LaCoO_3$ was made by Marquis & Sis (1977). The APB is rather ill defined and has a serrated appearance; such serrations could also be modelled, as shown in Fig. 6(*b*).

Side-stepping bismuthate layers

Fig. 7 is another image from the same fragment. Here the features *CD*, *EF*, *GH*, *IJ*, *etc.* represent shifts, of one octahedron width, sideways, of the Bi_2O_2 layers. These shifts do not appear to be aligned exactly along the [110] direction, there being bands of overlap contrast similar to those observed in complex niobium oxides (Hutchison, Lincoln & Anderson, 1974). A schematic drawing of such a fault is shown in Fig. 8. It is not possible to locate precisely the position of the step along the [110] direction on the basis of a single image. Nevertheless, the contrast clearly indicates the presence of this feature in the crystal. The perovskite sublattice is largely unaffected by these sidesteps; the rows of *A*-site cations can be traced perfectly across the steps. Occasional kinks such as indicated by an arrow in Fig. 7 probably arise from dislocations; these are discussed below.

Superdislocations – extra perovskite slabs

Terminating slabs of perovskite structure, with associated extra Bi_2O_2 layers, are occasionally observed. An example of the inclusion of a single extra slab

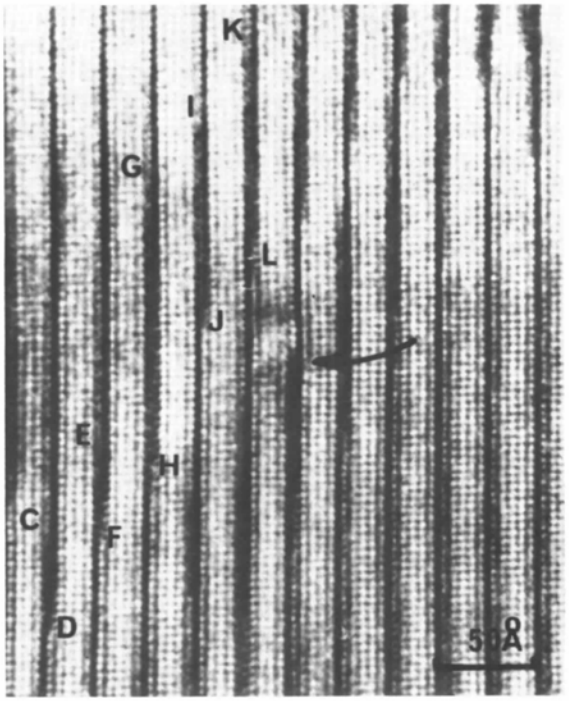

Fig. 7. Early 500 kV image of $Ba_2Bi_4Ti_5O_{18}$. Features *CD*, *EF*, *GH*, *IJ*, *etc.* are discussed in the text. The arrow indicates a possible dislocation.

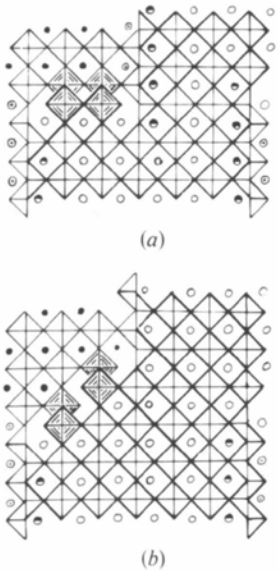

Fig. 6. (*a*) Idealized model for the antiphase boundary imaged in Fig. 5. Symbols are the same as in Fig. 1. (*b*) Possible structure of part of a serration along the antiphase boundary of Fig. 5.

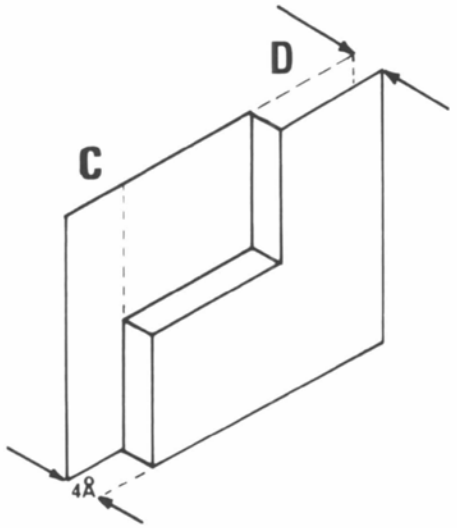

Fig. 8. Schematic model of feature *CD*, which is effectively a step or jog or a Bi_2O_2 layer, perpendicular to [110].

is shown in Fig. 9. Because of the antiphase relationship in which adjacent perovskite slabs are held, it can be shown that, when there is an odd number of extra slabs, the sublattice must contain dislocations containing both edge and screw components; when there is an even number of slabs there need not be any perturbation of the perovskite sublattice. Most of the strain associated with the defect shown in Fig. 9 is accommodated by progressive sidestepping of the bismuthate layers; the defect may in effect be regarded in terms of a dislocation of the bismuthate superlattice, superimposed upon the perovskite grid. Single unit-cell sideways shifts of the Bi_2O_2 layers similar to those shown in Fig. 7 are seen in the right-hand half of this micrograph (arrows). The structure of such steps is depicted in Fig. 10(*a*), confirming the model proposed previously by Hutchison *et al.* (1975, 1977). An alternative model (Fig. 10*b*), proposed by Horiuchi *et al.* (1977), for a similar defect in the closely related compound $Bi_7Ti_4NbO_{21}$, seems less likely, as it includes a large channel at the step, which would appear in the image as a bright dot or blob; such features were not observed in the micrographs.

Low-angle domain boundary dislocations

In the earlier study (Hutchison *et al.*, 1977) it was suggested that 180° domain walls could appear as low-angle boundaries in $Ba_2Bi_4Ti_5O_{18}$ and other related ferroelectrics. Such a low-angle domain boundary is shown in Fig. 11, across which the rotational displacement is about $2\frac{1}{2}°$. In this image all the cation positions are again resolved, the oxygen sites showing as white dots. The boundary contains a series of dislocations which accommodate the misfit; the core regions of these defects are enclosed by circles in Fig. 11. Analysis of these regions indicates that they contain an extra, terminating row of octahedra (and associated *A* cations), as shown in schematized form in Fig. 12. It is not possible to define the atomic configuration within the core itself with certainty. However, we are confident that there is indeed an extra octahedron row, as indicated, in each encircled region of Fig. 11. The earlier 100 kV study revealed small-angle boundaries which were interpreted as 180° domain walls; with the increased resolution employed in the present paper we are able to demonstrate that such boundaries contain dislocations. The movement of these dislocations through the crystal would be a means of accommodating the lattice distortions* which are known to accompany ferroelectric transitions (Cummins & Cross, 1967). In Fig. 11 the apparent image clarity is markedly different on either side of the boundary; in the upper part of the micrograph the crystal is evidently well aligned with [110] parallel to the electron beam

* In the Aurivillius phases, ferroelectric transitions can occur at relatively low temperatures: thus, for $Ba_2Bi_4Ti_5O_{18}$, the ferroelectric temperature is 590 K. This may be readily attained in the electron microscope as a result of localized heating of the specimen by the electron beam.

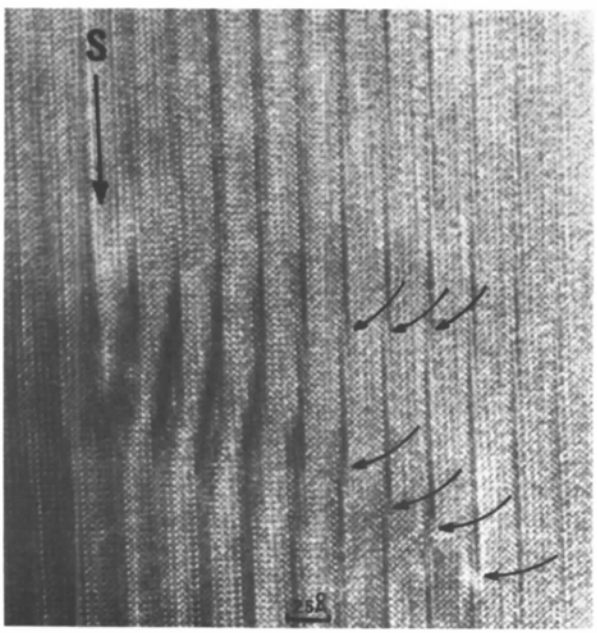

Fig. 9. Inclusion of an extra slab (*S*) of perovskite structure in $Ba_2Bi_4Ti_5O_{18}$. Note the progressive sidestepping of Bi_2O_2 layers (arrows) by means of which it is accommodated.

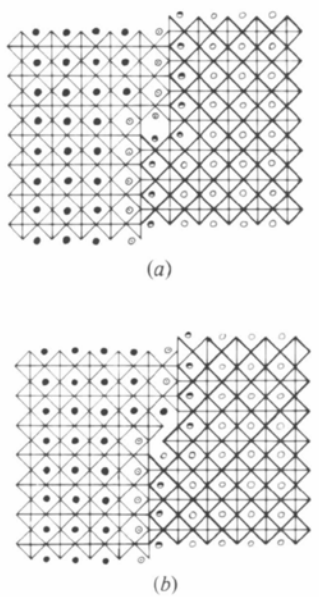

Fig. 10. (*a*) Detailed structure of unit-cell steps in Bi_2O_2 layers, as proposed by Hutchison *et al.* (1975). (*b*) Model for similar feature, as proposed by Horiuchi *et al.* (1977).

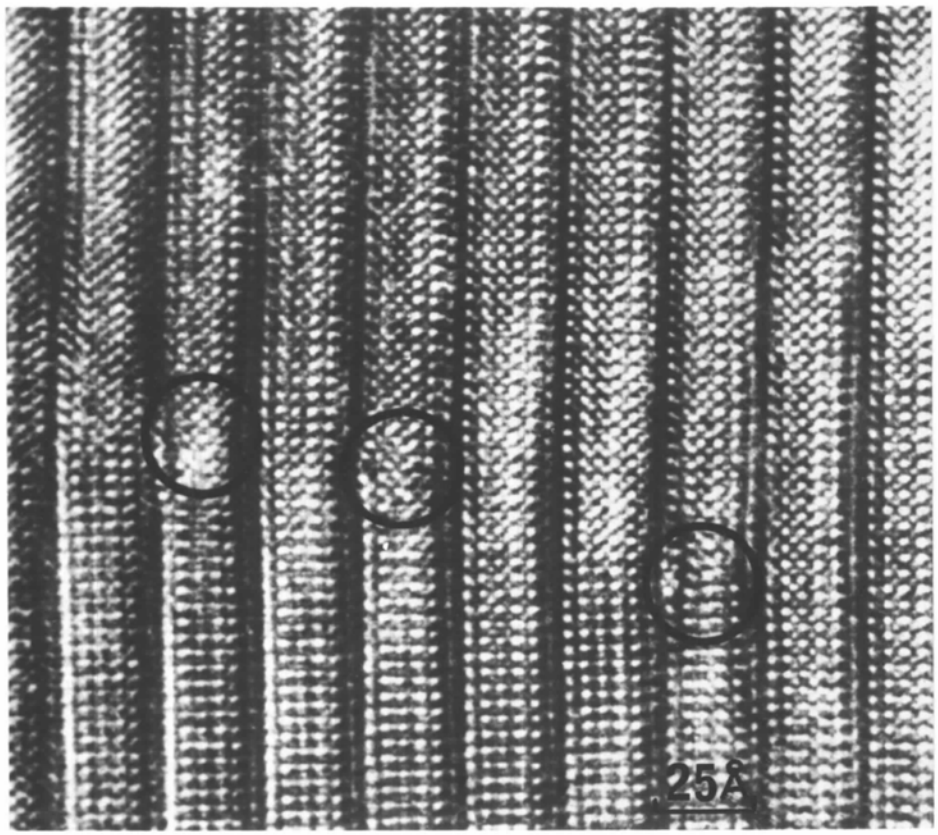

Fig. 11. Low-angle ($2\frac{1}{2}°$) domain boundary in $Ba_2Bi_4Ti_5O_{18}$. Along the boundary a series of dislocations occurs—core regions are enclosed by circles.

whereas in the lower, left part of the figure there is a slight tilt of the lattice away from this position and the cation sites are less clearly resolved. This could again be the result of lattice distortion around the dislocations.

Discussion

With the recent availability of improved performance in high-resolution electron microscopes we have been able to demonstrate that structure images could be obtained from the ferroelectric $Ba_2Bi_4Ti_5O_{18}$ which show detail of the crystal lattice at the atomic level. A resolution of about 2·5 Å was sufficient to resolve all the projected cation positions in the lattice. Images have been recorded of a variety of lattice defects, from which it has been possible to postulate structural models of these defects, and the way in which they are accommodated in the lattice. The feasibility of carrying out image calculations in support of these interpretations was considered. However, in view of the magnitude of the unit cell involved for perfect structure matching and, more particularly, in view of the complexity of the defect models concerned, it was decided not to attempt this at present. As demonstrated, the good agreement between image contrast and perfect structure (Fig. 3) provided adequate confidence for our image interpretation of crystals containing defects.

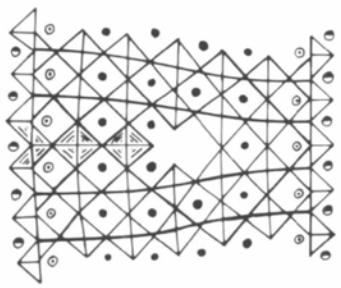

Fig. 12. Idealized representation of a dislocation core of the type encircled in Fig. 11.

By extending these experimental studies to related structures it is hoped to establish whether such lattice defects are more generally characteristic of these materials, and hence, eventually, to gain more insight into the macroscopic properties and behaviour of such materials.

The authors thank the Science Research Council for its support of this work, including the construction of the Cambridge University 600 kV high-resolution electron microscope, as a joint project between the Cavendish Laboratory and the Department of Engineering, and for subsequent personal support. Laboratory facilities in Oxford were provided by Professor Sir Peter Hirsch FRS. The assistance of Mr E. Watanabe during the commissioning of the Oxford JEM 200CX is also appreciated.

References

AHMED, H. & BROERS, A. N. (1972). *J. Appl. Phys.* **43**, 2185–2192.

AURIVILLIUS, B. (1949). *Ark. Kemi.* **1**, 463.

BANDO, Y., WATANABE, A., SEKIKAWA, Y., GOTO, M. & HORIUCHI, S. (1979). *Acta Cryst.* A**35**, 142–145.

BOYES, E. D., WATANABE, E., SKARNULIS, A. J., HUTCHISON, J. L., GAI, P. L., JENKINS, M. L. & NARUSE, M. (1980). In *Developments in Electron Microscopy and Analysis* 1979, edited by T. MULVEY, pp. 445–448. Bristol & London: Institute of Physics.

BURSILL, L. A. & HYDE, B. G. (1972). *J. Solid State Chem.* **4**, 430–446.

COSSLETT, V. E. (1980). *Proc. R. Soc. London Ser. A*, **370**, 1–16.

COSSLETT, V. E., CAMPS, R. A., SAXTON, W. O., SMITH, D. J., NIXON, W. C., AHMED, H., CATTO, C. J. D., CLEAVER, J. R. A., SMITH, K. C. A., TIMBS, A. E., TURNER, P. W. & ROSS, P. M. (1979). *Nature (London)*, **281**, 49–51.

CUMMINS, G. E. & CROSS, L. E. (1977). *Appl. Phys. Lett.* **10**, 14.

DIETRICH, I., FOX, F., KNAPEK, E., LEFRANC, G., NACHTRIEB, K., WEYL, R. & ZERBST, H. (1977). *Ultramicroscopy*, **2**, 241–249.

HORIUCHI, S., KIKUCHI, T. & GOTO, M. (1977). *Acta Cryst.* A**33**, 701–703.

HORIUCHI, S., MATSUI, Y., BANDO, Y., KATSUTA, T. & MATSUI, I. (1978). *J. Electron Microsc.* **27**, 39–48.

HUTCHISON, J. L. (1979). *Chem. Scr.* **14**, 181–186.

HUTCHISON, J. L., ANDERSON, J. S. & RAO, C. N. R. (1975). *Nature (London)*, **255**, 541–542.

HUTCHISON, J. L., ANDERSON, J. S. & RAO, C. N. R. (1977). *Proc. R. Soc. London Ser. A*, **355**, 301–312.

HUTCHISON, J. L., LINCOLN, F. J. & ANDERSON, J. S. (1974). *J. Solid State Chem.* **10**, 312–322.

KOBAYASHI, K., SUITO, E., UYEDA, N., WATANABE, M., YANAKA, T., ETOH, T., WATANABE, H. & MORIGUCHI, M. (1974). In *Electron Microscopy* 1974, edited by J. V. SANDERS & D. J. GOODCHILD, Vol. 1, pp. 30–31. Canberra: Australian Academy of Science.

MARQUIS, P. M. & SIS, L. B. (1977). *J. Mater. Sci.* **12**, 1484–1486.

NIXON, W. C., AHMED, H., CATTO, C. J. D., CLEAVER, J. R. A., SMITH, K. C. A., TIMBS, A. E., TURNER, P. W. & ROSS, P. M. (1977). In *Developments in Electron Microscopy and Analysis* 1977, edited by D. L. MISELL, pp. 13–16. Bristol & London: Institute of Physics.

Acta Cryst. (1981). A**37**, 125–130

Secondary Processes Accompanying X-ray Diffraction. Thermal Diffuse Scattering

BY A. M. AFANAS'EV

I.V. Kurchatov Institute of Atomic Energy, Moscow, USSR

AND S. L. AZIZIAN

Yerevan State University, Yerevan, Armenian SSR, USSR

(*Received* 10 *October* 1978; *accepted* 18 *May* 1980)

Abstract

A general formulation of the theory of the secondary radiation yield by X-ray diffraction in a crystal is given which enables such processes as photoelectric effect, fluorescence and thermal diffuse scattering (TDS) to be described in a unified way. Expressions describing TDS by crystals are obtained with an account of their elastic properties. TDS specificity is analyzed in detail. It is shown that the TDS yield curves are determined not only by the scattering cross sections for the incident and diffracted waves, but also by the phase relations between the scattering amplitudes.

0567/7394/81/010125-06$01.00

1. Introduction

In the last 10–15 years, the study of the angular dependence of secondary radiation yields, *i.e.* for